Density of Configurational States from First-Principles Calculations: The Phase Diagram of Al–Na Surface Alloys

Mikael Borg,[b, c] Catherine Stampfl,*[a, c] Anders Mikkelsen,[b] Johan Gustafson,[b] Edvin Lundgren,[b] Matthias Scheffler,[c] and Jesper N. Andersen[b]

The structural phases of Al_xNa_{1-x} surface alloys have been investigated theoretically and experimentally. We describe the system using a lattice-gas Hamiltonian, determined from density functional theory, together with Monte Carlo (MC) calculations. The obtained phase diagram reproduces the experiment on a quantitative level. From calculation of the (configurational) density of states by the recently introduced Wang–Landau MC algorithm, we derive thermodynamic quantities, such as the free energy and entropy, which are not directly accessible from conventional MC simulations. We accurately reproduce the stoichiometry, as well as the temperature at which an order–disorder phase transition occurs, and demonstrate the crucial role, and magnitude, of the configurational entropy.

A most challenging and important goal of materials science is to achieve an ab initio atomistic description of solids and their surfaces that can predict phenomena and properties occurring on macroscopic length and long timescales. Such methods should quantitatively describe measurable properties without relying on experimental parameters, which implies that they have to start ab initio, that is, from the self-consistent evaluation of the electronic structure. Recently, theoretical ab initio methods for achieving a unification of length- and timescales are being actively tested and developed for a variety of systems (see, e.g., ref. [1,2]). Herein, we apply and extend such methods to study the ordering of two-dimensional (2D) Al_xNa_{1-x} surface alloys. Our approach is quite general and offers a systematic and efficient procedure for reliably investigating (or "screening") the configurational space of materials surfaces as a function of temperature (T) and number of adatoms (or stoichiometry, x).

We describe the surface alloy system by a lattice-gas Hamiltonian (LGH) using interatomic interaction energies derived from density functional theory (DFT) calculations,[3–7] together with Monte Carlo (MC) simulations (called "ab initio LGH+MC"). Once the LGH has been constructed, one has at hand a fast and flexible tool to provide the energies of arbitrary system configurations. By comparison to new experimental data, we firstly show that this description accurately predicts the ordering of the alloy versus the Na concentration and temperature. Secondly, we use the MC algorithm recently introduced by Wang and Landau[8, 9] to calculate the "configurational" (or "structural") density of states (CDOS) for the Al_4Na composition of the surface alloy. Using the CDOS we then calculate the free (and internal) energy, configurational entropy, and specific heat. We show that this approach provides an accurate description of the temperature-induced order–disorder transition. To our knowledge, this is the first ab initio application of this method. Our calculations demonstrate how a very general treatment, as a function of x and T, can indeed be achieved.

The experiments were performed at beamline I311[10] at the MAX II synchrotron radiation facility, Lund, Sweden. The Al(100) crystal was mounted, cleaned and checked for contaminants as previously described.[11] Sodium was deposited from a carefully outgassed SAES source. Sodium coverages (θ_{Na}) were monitored via the Na-2p photoemission signal using the ($\sqrt{5}\times\sqrt{5}$)R27° structure (see Figure 1a) which forms for a coverage of 0.2 monolayers (ML)[11] (hereafter denoted $\sqrt{5}$) and the c-(2×2) structure (see Figure 1b) which forms for a coverage of
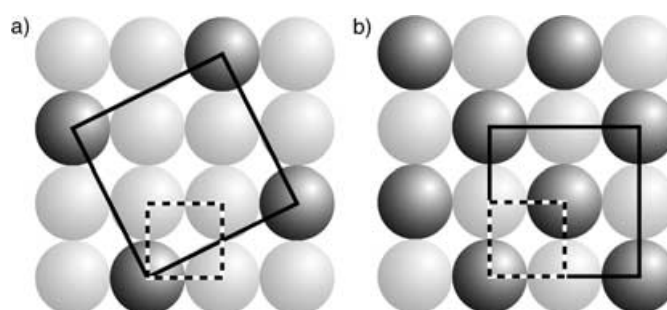
Figure 1. Atomic geometries of the a) ($\sqrt{5}\times\sqrt{5}$)R27° and b) c(2×2) phases. Dark and light cirles represent the Na and Al atoms, respectively. The Na atoms occupy surface Al sites. The missing Al atoms are assumed to be rebonded at kink sites at steps. The surface unit cell of the superstructures (——) and that of the Al(100) substrate (-----) are indicated.

[a] Prof. C. Stampfl
School of Physics, The University of Sydney
Sydney 2006 (Australia)
Fax: (+61) 2-935-17726
E-mail: stampfl@physics.usyd.edu.au

[b] Dr. M. Borg, Dr. A. Mikkelsen, J. Gustafson, Dr. E. Lundgren, Prof. J. N. Andersen
Department of Synchrotron Radiation Research
Institute of Physics, Lund University, P.O. Box 118, 221 00 Lund (Sweden)

[c] Dr. M. Borg, Prof. C. Stampfl, Prof. M. Scheffler
Fritz-Haber-Institut der Max-Planck-Gesellschaft
Faradayweg 4–6, 14195 Berlin (Germany)

0.5 ML,[12–14] as calibration points. [One monolayer = the number of Al atoms in a (100) plane]. Low energy electron diffraction (LEED) patterns were recorded with a video camera.

The Al_xNa_{1-x} alloys were prepared by deposition of submonolayer Na coverages on an Al(100) surface at temperatures around 300 K. At this temperature, Na atoms kick out and substitute Al atoms in the outermost Al(100) layer[11–14] at all but the lowest coverages (i.e., for $\theta_{Na} \leq 0.1$ ML Na atoms occupy fourfold coordinated hollow sites), resulting in the formation of an Al_xNa_{1-x} surface alloy. The kicked-out Al atoms are assumed to rebond at kink sites at steps on the surface whereby they gain the bulk cohesive energy.[15] Due to the immiscibility of Na in bulk Al, the Na atoms remain in the first Al(100) layer leading to a 2D nature of the alloy. After Na deposition, the LEED pattern was observed for temperatures ranging from ≈ 100 K to ≈ 350 K in order to map out the (θ_{Na}, T) phase diagram. The resulting phase diagram, which is consistent with previous results,[11–14,16] is shown in Figure 2 for θ_{Na} up to 0.5 ML. From the Al and Na core level binding energies, we conclude that substitutional adsorption of Na atoms occurs when θ_{Na} exceeds a critical value of about 0.1 ML.
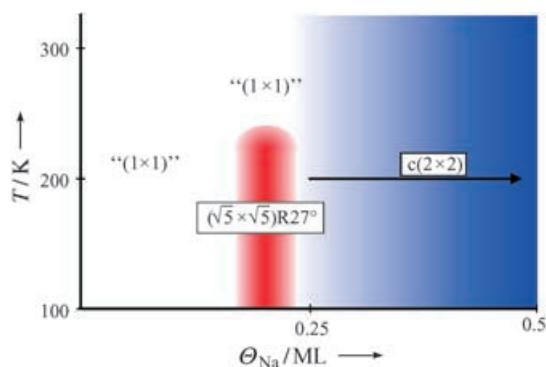
Figure 2. Experimental phase diagram. For the $\sqrt{5}$ structure, the red shading indicates the region of (T, θ_{Na}) space in which it exists. The blue shading indicates that the c(2×2) phase begins to form in patches on the surface, which become complete at $\theta_{Na} = 0.5$ ML. The label "(1×1)" indicates the disordered phase.

At low temperatures, three phases are detected: a "(1x1)" at low coverage (≤ 0.17 ML) indicating a disordered Na arrangement, a $\sqrt{5}$ phase at $\theta = 0.2 \pm 0.03$ ML,[11] and finally a c(2×2) phase in which the LEED spot intensity increases as θ_{Na} approaches 0.5 ML. The atomic structure of the latter two phases is shown in Figure 1. The experiments identify an order–disorder phase transition in the temperature range of 220–300 K, in which the ordered $\sqrt{5}$ structure changes to a disordered phase with the Na atoms still occupying substitutional sites. Correspondingly, the LEED pattern changes from a $\sqrt{5}$ superstructure to a "(1×1)" pattern, indicative of the disordered phase. [We note that the perfectly ordered clean Al(100) surface gives rise to sharp (1×1) LEED spots; the disordered arrangement of Na on Al(100) also gives rise to a (1×1) pattern, but the spots are diffuse—hence the label "(1×1)"]. On cooling,

the $\sqrt{5}$ structure is once again observed; that is, the transition is reversible.

In Figure 3 we show for $\theta_{Na} = 0.2$ ML, the ratio of the integrated intensities of the fractional and integer $\sqrt{5}$ order LEED spots for an incident electron energy of 82 eV versus temperature (similar results were obtained at other energies).
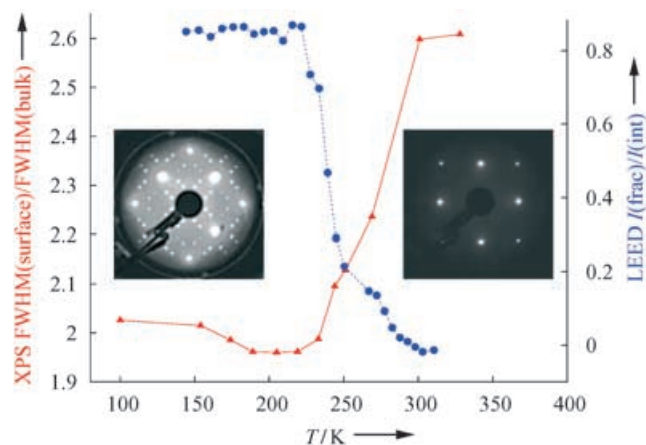
Figure 3. Full-width-at-half-maximum (FWHM) of the Al-2p peak from Al atoms in the first layer relative to the FWHM of the Al-2p bulk emission (▲, left ordinate, red) and the fractional/integer order intensity ratio as a function of temperature (●, right ordinate, blue). The insets show the LEED patterns of the $\sqrt{5}$ phase (left) and the "(1×1)" disordered phase (right).

The loss of long-range order, initiated at temperatures above ≈ 225 K, is evident from the strong decrease in the relative fractional order intensity above this temperature (Figure 3, ■). As previously discussed,[11] the order–disorder transition also manifests itself in Al-2p photoemission spectra. Briefly, in the ordered $\sqrt{5}$ overlayer, each first layer Al atom is coordinated to one Na atom (see Figure 1a) resulting in a single shift of the Al-2p binding energy for these Al atoms. In the disordered alloy, however, the Al to Na coordination is different for different Al atoms, resulting in a distribution of individual Al-2p shifts which cannot be resolved.[11] Instead they cause an abrupt increase in the width of the Al-2p emission as the surface alloy disorders. In Figure 3 (▲) we show new measurements of this temperature-dependent broadening. In order to approximately correct for broadenings induced by other effects (see, e.g., ref. [17]) the values given are the ratio between the full width at half maximum (FWHM) of the Na induced, and the bulk emission peaks, respectively. As core-level shifts in metallic systems are dominated by short-range, local effects,[17] the strong increase demonstrates that short-range order is also lost in the order–disorder transition. In summary, the studied system is a two-dimensional surface alloy with an ordered phase at low temperature and a disordered phase at elevated temperatures at the particular stoichiometry $x = 0.2$. In the following we will show how we can describe this system from first-principles calculations—also at elevated temperatures—by combining state-of-the-art DFT calculations with a novel MC algorithm.

Theoretically we describe the system as a 2D lattice-gas consisting of the Al and Na atoms in the alloy layer, adsorbed on the Al(100) crystal. We can thus map the (lateral) atomic Na and Al positions of the alloy to the fourfold hollow sites of the underlying square (100) lattice. This does not mean that we disregard out-of-plane relaxations, or that we keep the geometry of the underlying Al(100) plane fixed. Indeed, the DFT calculations used for extracting the interaction energies involve full geometrical optimization. The lattice-gas Hamiltonian (LGH) is written as shown in Equation (1):

$$H = V^1 \sum_1 n_i + \sum_{m=1}^{6} V_m^2 \sum_{\langle ij \rangle_m} n_i n_j + \sum_{m=1}^{2} V_m^3 \sum_{\langle ijk \rangle_m} n_i n_j n_k$$
$$+ V^4 \sum_{\langle ijkl \rangle} n_i n_j n_k n_l \tag{1}$$

where V^1 is the adsorption energy for an isolated Na atom (including the vibrational contribution)[18], n_i are the occupation numbers and equal 0 or 1 depending on whether a site is empty or occupied, respectively, and V_m^2 (V_m^3, V^4) are the two-(three-, four-) body interaction energies. In principle, the expansion of the LGH is infinite, however, in practice it can be truncated. In particular, the choice of parameters was obtained from an unbiased testing using the cross-validation scheme. From this, we could conclude that using up to four-body terms gives sufficient accuracy for a proper description of the system. We note that the number and type of interactions for the present Na/Al(100) system are larger than those that were used for studying O/Ru(0001);[3] this is mainly due to the far-reaching Na–Na interactions and notable disruption of the substrate due to the Al vacancies.

The DFT calculations,[19,20] were performed using a plane-wave basis set, norm-conserving pseudo-potentials,[21,22] and the generalized gradient approximation .[23] We used a super-cell approach, with slabs seven atomic layers thick, separated by a vacuum region that corresponds to eight Al layers. The Na atoms were placed on one side of the slab and a dipole correction was employed to take into account the dipole that is thus induced.[21] The first two layers, that is, the surface alloy and the first Al(100) layer, were fully optimized with respect to the atomic positions so that the forces on atoms in these layers were less than 0.025 eV Å^{-1}. We used a highly accurate **k**-point mesh for Brillouin Zone (BZ) integrations, corresponding to 78 **k**-points in the irreducible BZ of the (1×1) surface unit cell. This allowed us to use exactly the same **k**-points for all of the surface structures studied. This is essential for determining the adsorption energies of different coverages, as calculated in different supercells, to the required high numerical accuracy. The adsorption energies are then used to derive the interaction parameters. Our calculations show that substitutional adsorption (Na occupying an Al site) is preferred over adsorption in hollow sites (Na in a fourfold-coordinated site on the Al(100) surface) by 0.07 eV, 0.23 eV, and 0.2 eV, for Na coverages $\theta_{Na} = 0.111$ (1/9) ML, 0.2 ML (the $\sqrt{5}$ phase), and 0.5 ML [the c(2x2) phase], respectively. For the low coverage of 0.0625 (1/16) ML, we find that hollow site adsorption is favorable (by

0.0046 eV), in accordance with experiment. Thus, the calculations predict that for low coverage (<0.0625 ML), the hollow site is slightly preferred, while for higher coverages, the Na atoms will occupy the substitutional site, providing energy activation barriers can be overcome.

The Na adsorption energy, E_{ad}, for a structure s with N Na atoms in the unit cell was calculated under the assumption that the expelled Al atoms adsorb at kink sites at steps, whereby they gain the bulk cohesive energy.[15] Thus, Equations (2) is valid,

$$E_{ad} = (E_S + N \cdot E_{Al\,bulk}) - (E_S^{Al} + N \cdot E_{Na\,atom}) \tag{2}$$

where E_S is the total energy of the relaxed structure, $E_{Al\,bulk}$ the energy of a bulk Al atom, E_S^{Al} the clean aluminum slab with the same unit cell, and $E_{Na\,atom}$ the energy of a free Na atom.

We performed calculations for 25 different Na/Al(100) configurations, with coverages ranging from 0.0625 to 0.5 ML. In order to construct the LGH, we used leave-many-out cross-validation (LMO-CV)[24,25] to select a set of parameters with high, predictive capabilities. This approach represents an unbiased way to select the relevant interaction parameters. Briefly, in the LMO-CV approach, the structures calculated by DFT are divided into two groups, namely, one containing $M–d$ structures and the other containing d structures, where M is the total number of structures calculated ($M = 25$) and d is an arbitrary fraction of the total (here $d = 3$ and 5). The group $M–d$ is used in a least-squares-fit to obtain the interaction parameters, and the remaining d structures are used to calculate the "prediction error" (i.e., the root-mean-square of the deviations between the energies obtained by the LGH and DFT). This is then repeated for many random divisions (into groups $M–d$ and d) of the total set M. The average prediction errors can then be used to compare the predictive powers of different sets of interaction parameters. For example, including more or less pair (two-body) interactions, or more or less, or different trio (three-body) interactions.

The LGH that we obtain using the results from the LMO-CV (with $d = 3$, 5 and $M = 25$) includes two-body (or pair) interactions between the Na atoms up to the 6th nearest neighbor, two types of three-body (or trio) interactions, and one four-body (quarto) interaction. In particular, linear and triangular trio interactions with a distance of a_0 between the Na atoms, where a_0 is the lattice constant of the face centered cubic (fcc) lattice. Similarly, the four-body interaction consists of a square arrangement of Na atoms of size a_0^2. These interactions are sketched in Figure 4 and the values are listed in Table 1. In general, the pair interactions are all repulsive and decrease in magnitude with increasing separation of the Na atoms. This is, as expected, based on the simple picture that the Na atoms are partially positively charged on the Al substrate so that they will experience an electrostatic repulsion. The trio interactions, however, are attractive and have a stabilizing effect. More dense trio interactions (i.e., Na atoms arranged at nearest-neighbor lattice sites, instead of next nearest-neighbor sites) are highly repulsive and thus not relevant. Further details will be presented in a forthcoming publication.[26]
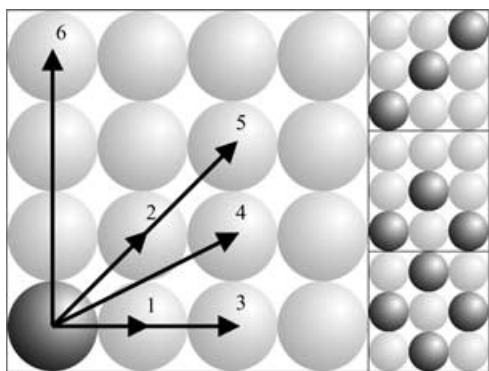
Figure 4. Sodium–sodium interactions included in the LGH: pair interactions (V_i^2 with $i = 1$–6) to the left, and the two trio interactions (V_i^3) and quarto interaction (V_1^4) to the right. The arrows labeled 1–6 indicate the six pair (two-body) interactions between the dark shaded atom, and the atom at the head of the arrow. The numerical values are given in Table 1.

Table 1. Interaction parameters for the Na/Al(100) system as sketched in Figure 4: $V_{m=1,6}^2$ are the pair interactions, $V_{n=1,2}^3$ are the trio interactions, and V_1^4 is the quarto interaction. A positive value indicates a repulsive interaction and a negative value an attractive interaction between the Na atoms. The unit is eV.

V_1^2	V_2^2	V_3^2	V_4^2	V_5^2	V_6^2	V_1^3	V_2^3	V_1^4
0.305	0.107	0.082	0.018	0.024	0.018	−0.058	−0.063	0.142

Adsorption energies calculated using direct DFT and the LGH with the parameters in Table 1 agree very well: the root-mean-square (rms) error in the fit is 14.3 meV per sodium adsorbate. We note that other parameter sets can yield similar rms fit errors, and in general, the more parameters the lower they become. This can be a result of over-fitting and not a reflection that the parameter set is better. The "prediction error" of the LMO-CV is the more appropriate indicator of the quality of the interactions.

First, using standard MC-simulated annealing we searched for stable 0 K structures at different coverages by starting with random configurations at elevated temperatures and then slowly cooling the system. For $T > 0$ K simulations, we started from the 0 K structure and then performed MC steps until the energy of the system was converged. For this, (80×80) lattices were used. Simulations with smaller lattices yielded very similar results, indicating that our lattice is sufficiently large. For the $T = 0$ K ground-state configurations, we find a series of large-unit-cell structures for $\theta_{Na} < 0.18$ ML. These are not relevant in that they represent only very shallow minima in the energy landscape and on heating slightly, these features disappear. In the range 0.18 ML $< \theta_{Na} < 0.26$ ML a $\sqrt{5}$ structure occurs, and for θ_{Na} from 0.26 to 0.5 ML, we find structures whose Fourier transformation shows a predominant c(2×2) ordering with additional "longer-range" structure. In agreement with experiment, the simulations do not yield a p(2×2) ground-state structure for 0.25 ML at any T. This can be primarily traced back to the relatively large third-neighbor pair interaction. For $T > 0$ K, the c(2×2) ordering is maintained in the studied temperature range considered, whereas the more "long-range" ordering

weakens considerably. This is all consistent with the experimentally observed structures above 100 K (see Figure 2). Our calculations also find that the $\sqrt{5}$ structure disorders above 300 K in close agreement with experiment.

Because the standard metropolis scheme is rather inefficient for finding phase transition temperatures, extracting the specific heat, and directly determining the free energy and entropy, we have employed the MC algorithm of Wang and Landau,[8, 9] which affords an accurate evaluation of the (configurational) density of states (CDOS), $g(E)$, that is, the number of system configurations with a certain energy, E. From $g(E)$ all major thermodynamic functions can be directly calculated. In particular, we apply this to investigate in more detail the order–disorder transition at coverage 0.2 ML. While most conventional MC algorithms, such as the "metropolis importance sampling",[26] generate a canonical distribution, $g(E)e^{-E/k_BT}$, at a given temperature, the Wang–Landau formalism focuses instead on obtaining an accurate estimate of $g(E)$, which is independent of temperature. This is achieved by performing a random walk in "energy space". From $g(E)$ all major thermodynamic functions can be directly determined, for example, the free energy and entropy—quantities that are not directly accessible by conventional MC. In the Wang–Landau approach, the configurational space is sampled with the probability $g(E)^{-1}$. An initial CDOS of $g^i(E)$ is then modified until the sampling rates of the energy intervals are equal. For these simulations, we again used a (80× 80) lattice, unless stated otherwise. In Figure 5 a, the resulting CDOS is shown.
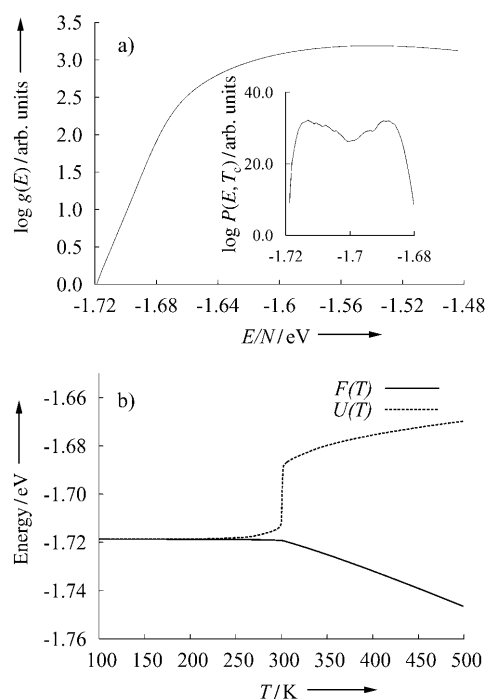
Figure 5. a) Density of (configurational) states (CDOS), $g(E)$, as a function of energy for $\theta_{Na} = 0.2$ ML. Inset: The logarithm of the canonical distribution $P(E,T) = g(E)e^{-E/k_BT}$, at the critical temperature, T_c. b) Free energy, $F(T)$, and internal energy, $U(T)$, as a function of temperature, derived from $g(E)$. The cusp in $F(T)$ and discontinuity in $U(T)$ at 301 K reflect the order–disorder phase transition, experimentally observed in the range 220–300 K, as shown in Figure 3.

From this we can calculate, for example, the canonical distribution at a given temperature, $g(E)e^{-E/k_BT}$, the free energy as given in Equation (3):

$$F(T) = -k_B T \ln \sum_E g(E)e^{-E/k_B T} = k_B T \ln(Z) \qquad (3)$$

where Z is the partition function, the internal energy shown in Equation (4):

$$U(T) = \langle E \rangle_T = \sum_E E g(E)e^{-E/k_B T}/Z \qquad (4)$$

the entropy [Eq. (5)]:

$$S = (U-F)/T \qquad (5)$$

and the specific heat, [Eq. (6)]:

$$C_v(T) = (\langle E^2 \rangle_T - \langle E \rangle_T^2)/T^2 \qquad (6)$$

As shown in Figure 5 b, at $T = 301$ K, the free energy exhibits a cusp and the simulated system undergoes a phase transition at this temperature. Thus, the simulations reproduce very nicely the experimental order–disorder phase transition. As an indication of the sensitivity to the interaction parameters, we note that a (uniform) $\pm 10\%$ change of the interaction parameters resulted in a change of the transition temperature of ± 25 K. Furthermore, as the adsorption energy of a single Na atom (V^1) does not change the shape of $g(E)$, but only its position on the energy axis, changes in V^1 (e.g., DFT-GGA typically overestimates the binding of adparticles to surfaces) do not affect the phase transition as a function of stoichiometry or temperature. The discontinuity of the internal energy at the transition temperature shows that the phase transition is of first order. The phase transition is also indicated by the double peak in the logarithm of the canonical distribution (Figure 5 a, inset) and as a singularity in the specific heat at the critical temperature shown in Figure 6. We note that the peaks in the latter plot are somewhat broadened and this is because we
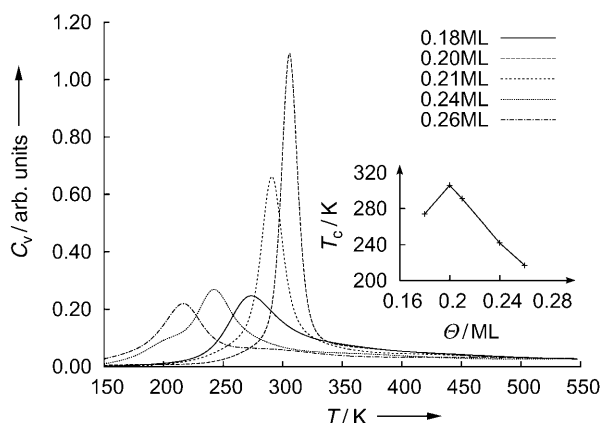
used a 20×20 lattice for these simulations involving various coverages; calculations using the 80×80 lattice for a coverage of 0.2 ML, exhibit a sharp peak at essentially the same temperature (i.e., the deviation is less than 2 K).

It can be noticed that the experimental phase transition occurs over a considerably wider temperature range than indicated by the simulations. A possible reason is that the atomic processes involved in the phase transition are kinetically hindered. For example, the necessary substantial atomic rearrangements involved for the diffusion of the substitutionally adsorbed Na atoms. Thus, it may be experimentally difficult to achieve full thermodynamic equilibrium on the applied measuring times. Furthermore, we also note that the experimental determination of the Na coverage is subject to some uncertainty. With regard to the latter, simulations at coverages slightly above or below 0.20 ML show a decrease in the critical temperature, as demonstrated by evaluation of the specific heat in Figure 6. Thus, any experimental nonuniformity of the coverage will induce a broadening of the phase transition, and deviations from 0.20 ML will cause a lowering of the critical temperature. We also note that steps play a decisive role in this phase transition, and will also affect the quality of the adlayer. However, the latter is not considered in the theoretical simulations.

From Figure 5 b it can be seen that the free energy decreases notably with increasing temperature after the phase transition occurs. The reason for this is clearly the entropic contribution S, the magnitude of which increases at the transition temperature and continues to increase steadily with temperature thereafter. Taking this configurational entropy into account is therefore (and obviously) the crucial aspect in the simulation and the understanding of this order–disorder phase transition, and the LGH+MC approach, with its proper sampling of configuration space, is the only method that can provide it.

In summary, using the "ab initio LGH+MC" approach we have determined the structural phase diagram of Al$_x$Na$_{1-x}$ surface alloys. The phase diagram agrees well with new experimental measurements for all stoichiometries and temperatures. Using the recently introduced MC algorithm of Wang and Landau, which yields an accurate estimation of the CDOS, we reproduce the experimental order–disorder phase transition and show the important role, and magnitude of, the configurational entropy. We expect that the theoretical method as demonstrated here may prove useful for the efficient screening and identification of new and unanticipated surface phases of materials.

Acknowledgements

Figure 6. Specific heat, $C_v(T)$, as a function of temperature as obtained from Wang–Landau MC simulations, at different Na coverages. Inset: Critical temperature T_c (as determined from the peak positions) for an order–disorder phase transition as a function of Na coverage.

[1] C. Stampfl, M. V. Ganduglia-Pirovani, K. Reuter, and M. Scheffler, *Surf. Sci.* **2002**, *500*, 368.

[2] K. Reuter, C. Stampfl, M. Scheffler in *Handbook of Materials Modeling*, *Vol. 1*: *Ab initio Atomistic Thermodynamics and Statistical Mechanics of Surface Properties and Functions* (Ed.: S. Yip), Kluwer, Dordrecht, **2005**.

[3] C. Stampfl, H. J. Kreuzer, S. H. Payne, H. Pfnür, M. Scheffler, *Phys. Rev. Lett.* **1999**, *83*, 2993.

[4] D. B. Laks, L. G. Ferreira, S. Froyen, A. Zunger, *Phys. Rev. B* **1992**, *46*, 12 587.

[5] D. de Fontaine in *Solid State Physics* (Eds.: H. Ehrenreich, F. Seitz, D. Turnbull), Academic Press, New York, **1979**, vol. 34, pp. 1.

[6] P. D. Tepesch, M. Asta, G. Ceder, *Modell. Simul. Mater. Sci. Eng.* **1998**, *6*, 787.

[7] G. Ceder, G. D. Garbulsky, P. D. Tepesch, *Phys. Rev. B* **1995**, *51*, 11 257.

[8] F. Wang, D. P. Landau, *Phys. Rev. Lett.* **2001**, *86*, 2050; *Phys. Rev. E* **2001**, *64*, 056 101.

[9] B. J. Schulz, K. Binder, M. Müller, D. P. Landau, *Phys. Rev. E* **2003**, *67*, 067 102.

[10] R. Nyholm, J. N. Andersen, U. Johansson, U. B. N. Jensen, I. Lindau, *Nucl. Instrum. Methods* **2001**, *467*, 520.

[11] M. Borg, A. Mikkelsen, M. Birgersson, M. Smedh, E. Lundgren, D. L. Adams, C.-O. Almbladh, J. N. Andersen, *Surf. Sci.* **2002**, *515*, 267.

[12] J. N. Andersen, E. Lundgren, R. Nyholm, M. Qvarford, *Phys. Rev. B* **1992**, *46*, 12 784.

[13] W. Berndt, F. Weick, C. Stampfl, A. M. Bradshaw, M. Scheffler, *Surf. Sci.* **1995**, *330*, 182.

[14] C. Stampfl, K. Kambe, R. Fasel, P. Aebi, M. Scheffler, *Phys. Rev. B* **1997**, *57*, 15 251.

[15] M. Scheffler, C. Stampfl in *Handbook of Surface Science, Vol. 2*: *Theory of Adsorption on Metal Substrates*, (Eds.: K. Horn, M. Scheffler), Elsevier, Amsterdam, **2000**.

[16] J. O. Porteus, *Surf. Sci.* **1974**, *41*, 515.

[17] J. N. Andersen, C.-O. Almbladh, *J. Phys. Condens. Matter* **2001**, *13*, 11 267.

[18] The vibrational contribution to the energy is obtained as follows: The "spring constants" for Al atoms in the bulk and in the surface layer are calculated, as well as for the isolated substitutional Na atoms, by fitting the "energy versus atomic-displacement curve" to a quadratic form. From this, one obtains the zero-point vibrations ($3/2\,h\omega$) for the different atoms. Finally, the difference in zero-point energies between that of the Na atom plus a bulk Al atom (adsorption system) and that of a surface Al atom (reference Al-surface) is made, and it is this energy which is added to the isolated Na adsorption energy, V^1. The resulting values are: 11 meV for Al bulk, 10.6 meV for an Al surface atom, and 3.8 meV for the isolated substitutional Na atom, yielding a correction of 3.4 meV to the isolated Na adsorption energy.

[19] P. Hohenberg, W. Kohn, *Phys. Rev.* **1964**, *136*, 864.

[20] W. Kohn, L. J. Sham, *Phys. Rev.* **1965**, *140*, 1133.

[21] M. Bockstedte, A. Kley, J. Neugebauer, M Scheffler, *Comput. Phys. Commun.* **1997**, *107*, 187.

[22] M. Fuchs, M. Scheffler, *Comput. Phys. Commun.* **1999**, *119*, 67.

[23] J. P. Perdew, K. Burke, M. Ernzerhof, *Phys. Rev. Lett.* **1996**, *77*, 3865.

[24] J. Shao, *J. Am. Stat. Assoc.* **1993**, *88*, 486.

[25] P. Zhang, *Ann. Math. Stat.* **1993**, *21*, 299.

[26] M. Borg, M. Todorova, C. Stampfl, M. Scheffler, unpublished results.

[27] N. Metropolis, A. W. Rosenbluth, M. N. Rosenbluth, A. H. Teller, E. Teller, *J. Chem. Phys.* **1953**, *21*, 1087.